Tapering enhanced stimulated superradiant amplification

2015 New J. Phys. 17 063036

(http://iopscience.iop.org/1367-2630/17/6/063036)

New Journal of Physics
The open access journal at the forefront of physics

Deutsche Physikalische Gesellschaft DPG
IOP Institute of Physics

Published in partnership with: Deutsche Physikalische Gesellschaft and the Institute of Physics

OPEN ACCESS

RECEIVED
13 February 2015

REVISED
29 April 2015

ACCEPTED FOR PUBLICATION
2 June 2015

PUBLISHED
29 June 2015

PAPER

Tapering enhanced stimulated superradiant amplification

J Duris[1], A Murokh[2] and P Musumeci[1]

[1] Department of Physics and Astronomy, UCLA, Los Angeles, CA, 90095, USA
[2] Radiabeam Technologies, Santa Monica, CA 90404, USA

E-mail: jduris@physics.ucla.edu

Keywords: laser particle acceleration, free electron laser, sideband suppression, extreme ultraviolet lithography, x-ray diffraction

Abstract

High conversion efficiency between electrical and optical power is highly desirable both for high peak and high average power radiation sources. In this paper we discuss a new mechanism based on stimulated superradiant emission in a strongly tapered undulator whereby a prebunched electron beam and focused laser are injected into an undulator with an optimal tapering calculated by dynamically matching the resonant energy variation to the ponderomotive decelerating gradient. The method has the potential to allow the extraction of a large fraction (~50%) of power from a relativistic electron beam by converting it into coherent narrow-band tunable radiation, and shows a clear path to very high power radiation sources of EUV and hard x-rays for applications such as lithography and single molecule x-ray diffraction. Finally, we discuss a technique using chicane delays to suppress the sideband instability, improving radiation generation efficiencies for interaction lengths many synchrotron wavelengths long.

1. Introduction

Among coherent radiation sources, free-electron lasers (FEL) carry unique advantages such as wavelength tunability and access to the short wavelength region of the electromagnetic spectrum. FELs are not limited by thermal or non-radiative loss mechanisms characteristic of atomic lasers based on solid state and gas phase gain mediums. Nevertheless, saturation effects limit the conversion efficiency to levels comparable with the Pierce parameter ρ which is typically <0.1% [1]. FEL undulator tapering [2] has been shown to allow much larger efficiencies. At very long wavelengths (35 GHz) where it is possible to use a waveguide to maintain an intense radiation field on axis, up to 35% conversion efficiency has been demonstrated [3]. At shorter wavelengths [4, 5], the reduction of gain guiding and the onset of spectral sidebands have limited the effectiveness of tapering [6]. For example at the LCLS, the power extraction has remained well below the percent level limiting the amount of energy in the pulse to a few mJ. Higher conversion efficiencies could lead to unprecedented intensity x-ray pulses with over 10^{13} photons per pulse providing sufficient signal-to-noise to enable the long sought goal of single molecule imaging [7]. In the visible and UV spectral ranges, large electrical to optical conversion efficiencies are also very attractive for the development of high average power (10–100 kW-class) lasers especially when considering that superconducting radio-frequency linacs can create relativistic electron beams with very high wall-plug efficiencies and MW average power.

In order to increase the electro-optical conversion efficiency, we note that the burgeoning field of laser accelerators is making extreme progress on the opposite problem—that is, optical to electrical power conversion. Among the various schemes for laser acceleration, the inverse free-electron laser (IFEL) accelerator is a far-field vacuum-based scheme which uses an undulator magnet to couple a transversely polarized radiation field to the longitudinal motion of the electrons [8]. The lack of nearby boundaries or a medium (gas, plasma) to couple the light to the electrons implies very little irreversible losses and in principle enables very high energy transfer efficiencies. Simulations show that an IFEL could be optimized to transfer 70% of optical power to a relativistic electron beam [9]. Recent experimental results demonstrated energy doubling of a 52 MeV beam with ~100 MeV m^{-1} average accelerating gradients and capture of up to 30% of an unbunched electron beam [10] using a

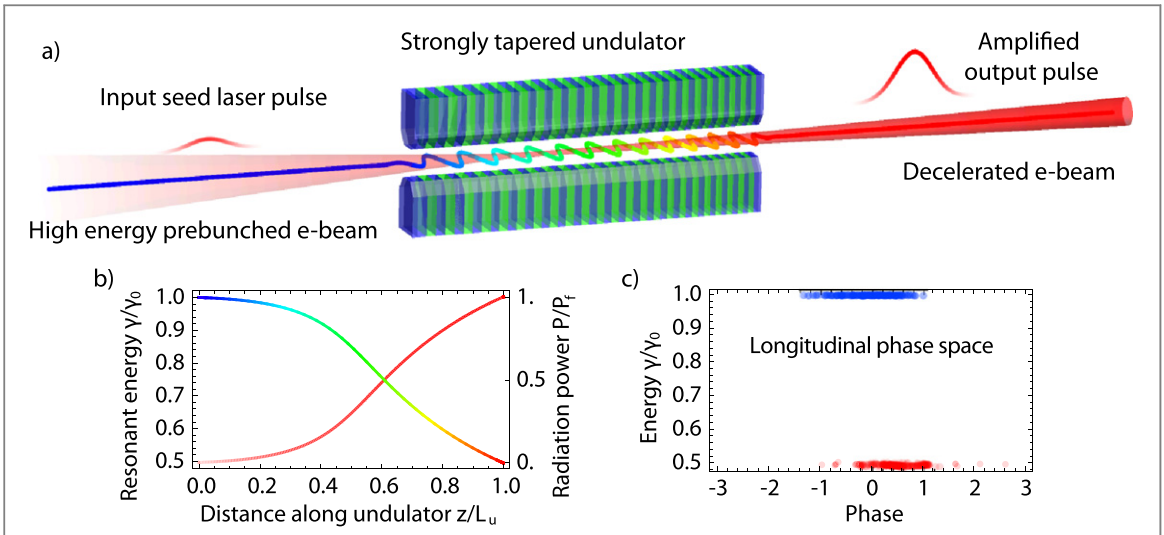

Figure 1. An implementation of TESSA. The diagram in (a) shows a seed laser focused into the strongly tapered undulator along with a prebunched electron beam. As the e-beam energy—blue represents high energy while red is low—decreases along the undulator, the laser power grows. Plots of (b) the normalized electron energy and laser power along the undulator and (c) initial and final longitudinal phase spaces are shown.

strongly tapered undulator in a helical geometry IFEL interaction. Reversing the process to decelerate a prebunched beam by the same mechanism, it would be in principle possible to transfer back to the drive laser half of the electron energy—effectively extracting 50% of the electron beam power and converting it into coherent radiation [11].

Based on this idea, we investigate in this paper a novel scheme for efficient generation of radiation whereby a high intensity seed laser pulse and a relativistic electron beam copropagate in a tapered undulator and the IFEL interaction is used to decelerate the beam. The scheme relies on the coherent emission of a prebunched beam going through an undulator in the presence of an intense driving field (i.e. stimulated superradiance emission [12]). Very strong tapering of the undulator is the other key ingredient to enable high conversion efficiencies and support large deceleration gradients and electron energy losses.

This tapering-enhanced stimulated superradiant amplification (TESSA) can be viewed as essentially an IFEL accelerator run backwards as a decelerator (see figure 1). The drive laser field stimulating the electron emission can be obtained from an external seed laser or, in a spectral region where external sources are not available, from redirecting FEL radiation into a TESSA afterburner undulator [13]. In this case, the FEL radiation can be refocused to reach peak intensities significantly larger than the FEL saturation level, thereby greatly increasing the initial decelerating gradient. In principle, it is also possible to obtain the seed pulse from the build-up in an oscillator cavity [14]. The required beam prebunching may be obtained by using the seed laser and a constant parameter undulator possibly in combination with one or more chicanes to apply R_{56} for larger bunching factors and reduced energy spread [15].

2. Tapering design

The TESSA particle dynamics in longitudinal phase space are best understood in the formalism of a high-gradient IFEL decelerator. We begin the analysis with the 1D FEL/IFEL equations [2] but limit the discussion to helical undulators as they offer at least twice the accelerating or decelerating gradient of planar ones [9]

$$\frac{\mathrm{d}\gamma}{\mathrm{d}z} = -\frac{kK_lK}{\gamma}\sin\psi \tag{1a}$$

$$\frac{\mathrm{d}\psi}{\mathrm{d}z} = k_w - k\frac{1+K^2}{2\gamma^2}. \tag{1b}$$

Here, γ is the particle energy in units of the rest energy m_0c^2 while $K = eB_0/m_0ck$ and $K_l = eE_0/m_0c^2k$ are respectively the undulator and laser field normalized vector potentials. $k = 2\pi/\lambda$ and $k_w = 2\pi/\lambda_w$ are the laser and undulator wavenumbers, and $\psi = (k_w + k)z - \omega t$ is the ponderomotive phase—that is, the phase of particles in the sinusoidal potential formed by the combined action of the laser and undulator fields on the electrons.

Resonant interaction requires a slowly varying ponderomotive phase ψ_r throughout the undulator. This is achieved by requiring $\mathrm{d}\psi/\mathrm{d}z = 0$ in equation (1*b*) for a resonant particle, leading to the resonance condition

$\gamma_r^2 = k(1 + K^2)/2k_w$. The resonant phase is a key parameter for the system and determines many properties of the longitudinal dynamics such as the gradient and the extent of the stable trapping area in the phase space (bucket). In general ψ_r is chosen around $\pi/4$ to maximize extraction efficiency, finding the best compromise between deceleration and detrapping.

Taking the derivative of the resonant condition, a decelerating gradient can then be determined from the variation in the undulator parameters along z:

$$\frac{\mathrm{d}\gamma_r^2}{\mathrm{d}z} = \frac{1}{2\lambda}(1 + K^2)\frac{\mathrm{d}\lambda_w}{\mathrm{d}z} + \frac{\lambda_w}{\lambda}K\frac{\mathrm{d}K}{\mathrm{d}z}. \tag{2}$$

For a given resonant phase ψ_r, there are different ways to optimize the tapering. For an undulator with constant period where $\mathrm{d}\lambda_w/\mathrm{d}z = 0$, setting the resonant energy gradient in equation (2) equal to the ponderomotive gradient in equation (1*a*) yields an equation for determining the optimum variation of K:

$$\frac{\mathrm{d}K}{\mathrm{d}z} = -2k_w K_l \sin\psi_r. \tag{3}$$

Changing the undulator period brings further advantages, both in flexibility (one can keep a larger K along the interaction), and in practical implementation since usually the magnetic field depends on the undulator period. Equating the right sides of equations (2) and (1*a*) for varying period yields

$$\frac{\mathrm{d}\lambda_w}{\mathrm{d}z} = -\frac{8\pi K_l K \sin\psi_r}{1 + K^2 + \lambda_w \mathrm{d}K^2/\mathrm{d}\lambda_w}. \tag{4}$$

This tapering equation can be solved once an undulator builder equation relating K to the undulator period λ_w is given. While there are many undulator designs which may relate these parameters, one particular design is a helical permanent magnet Halbach undulator with an undulator builder equation given by $K \cong \frac{e\lambda_w}{2\pi mc}1.8B_r\mathrm{e}^{-\pi g/\lambda_w}$, where g is the undulator gap and B_r is the remnant field of the magnets [16]. This specific undulator design is particularly useful and will be used in the examples below. Ultimately, the maximum energy extracted is limited by the feasibility of constructing an undulator with parameters matched to the resonance condition for the decelerated beam.

2.1. Low gain regime

In order to reach a better understanding of the TESSA dynamics, we start by analyzing the low-gain regime where the radiation power does not significantly change along the undulator. Defining the efficiency as the relative change in energy for the beam $\eta_{\mathrm{net}} = \gamma_f/\gamma_0 - 1$ and assuming $|\eta_{\mathrm{net}}| \ll 1$ for the constant period tapering case, we obtain an estimate of $\eta_{\mathrm{net}} \approx -2\pi N_w K_l \sin\psi_r$. In practice to reach tens of percent efficiency, the number of periods in the undulator N_w should be on the order of K_l^{-1}. This regime can be useful in an oscillator configuration (an analysis without undulator tapering is presented in [14]) where a small fraction of the output power is split and redirected at the input and the low gain is compensating the losses per pass. Note that if the injected electron beam is not prebunched, the first section of the interaction can be designed with $\psi_r \approx 0$ until full bunching occurs and the deceleration can start. Since the efficiency in the low-gain regime is independent of beam parameters, the output radiation power scales linearly with the input e-beam current. Considering diffraction, for a nearly constant undulator K, efficiency is maximized when a TEM_{00} Gaussian seed laser is focused with a Rayleigh range of $z_r \approx 0.15L_w$ to a waist at the undulator midpoint [9].

2.2. High gain regime

Whenever the stimulated superradiant emission becomes the dominant contribution to the total laser field driving the interaction, the undulator can be tapered more aggressively in order to take advantage of the additional ponderomotive drive. In this case, the tapering which maximizes conversion efficiency depends on the injected e-beam current since a higher current generates more radiation per unit length which allows larger decelerating gradients and higher electro-optical energy transfer rates. Thus, whereas the output radiation power scales linearly with injected current in the TESSA low gain regime, the output power in the high gain regime grows faster than linearly with respect to input e-beam current.

The main difference in calculating the tapering is that now K_l is the total electromagnetic field due to the seed plus the stimulated radiation, which is a dynamic variable evolving throughout the interaction and depending on the entire history of the e-beam spot size, current profile, and change in resonant energy throughout the interaction. The result is a complicated delay differential equation for K_l where three-dimensional (3D) effects play an important role. In this case, it is easier to optimize the undulator tapering by solving for the actual field evolution with the help of 3D simulations.

In practice, the well-benchmarked 3D FEL simulation code Genesis [17] is used to solve for the intensity of the radiation sampled by the electrons after a small number of undulator periods without tapering. This value is then fed into the tapering equation to calculate the optimum change of parameters for the following undulator section. These parameters along with the recorded particle and radiation distributions from the previous simulation are read by Genesis for the next step of the calculation which evolves the system for another small section of undulator. The optimization algorithm is then repeated until the end of the undulator. The result is an optimum undulator tapering and a self-consistent 3D simulation of the evolution of the electron beam and radiation in the optimized tapered undulator.

This tapering generation algorithm, dubbed Genesis-informed tapering or GIT, can be used both in the constant and the varying period cases. For the former, equation (3) is used to calculate the undulator K parameter variation while the period is held constant to the initially assigned value. For the variable period undulator, equation (4) is used where K is related to the period by the undulator builder equation.

It is of critical importance to choose the variation of the undulator parameters in order to maintain the majority of the particles trapped in the ponderomotive bucket. In particular due to 3D effects, not all particles experience the same laser intensity or K_l. In order to account for this problem, GIT looks up the local intensity seen by each macro-particle in the simulation and softens the tapering to keep any desired fraction of the beam trapped within the resonant bucket.

A particle maintains resonance if it is trapped near a local minimum of the ponderomotive potential. For particles with small relative energy deviations from resonance $\eta = \gamma/\gamma_r - 1$, the Hamiltonian can be approximately written as

$$H = ck_w\left(\eta^2 - \frac{2K_lK}{1+K^2}\left(\cos\psi + \cos\psi_r + (\psi + \psi_r - \pi\ \ \mathrm{sgn}\ \ \psi_r)\sin\psi_r\right)\right). \tag{5}$$

Particles in regions of phase space with $H < 0$ are trapped within the bucket, while particles outside of the bucket where $H > 0$ are free. It is important to note that the size and location of the bucket changes with the field sampled by each particle. Equation (5) is first evaluated for each particle with $\psi_r = 0$ to select particles with $H < 0$. We then determine the minimum K_l for this fraction of particles and use it with the tapering equations to determine the tapering of the undulator parameters.

With this method, it is helpful to start with a prebunched beam so that the tapering is allowed to change rapidly. Prebunching via the method of energy modulation with an undulator followed by R_{56} via a chicane or drift is greatly desirable here as it results in highly bunched beams with reduced energy spread, which increases ease of trapping by concentrating the injected e-beam in phase space. The use of a chicane also enables the e-beam bunches to be phase shifted to the center of the accelerating bucket. Furthermore, refocusing the driving radiation increases the bucket height, further decreasing the Hamiltonian and therefore increasing ease of trapping.

The advantages of prebunching and focusing the radiation before deceleration with TESSA help explain the advantages with respect to standard FEL tapering. The FEL mechanism fills the ponderomotive bucket at zero resonant phase so that only a relatively small core region of phase space may be matched into an accelerating bucket. Conversely, the TESSA approach tailors the input phase space to match well a strongly decelerating bucket from the beginning, allowing strong deceleration without sacrificing a significant fraction of the injected beam, and then optimizes the deceleration by matching the tapering and ponderomotive gradients while selecting the resonant phase in order to maximize trapping.

3. High power EUV light source

In the rest of this paper we examine the results of GIT for a couple of relevant cases where high extraction efficiency can enable break-through applications for electron beam-based light sources. In the first example we consider a 1 GeV linac-driven radiation source for EUV lithography, which requires achieving high average power at 13.5 nm. In a conventional SASE FEL optimized for this wavelength range, a practically achievable Pierce parameter is on the order of ~0.002, thus a state-of-the-art superconducting RF light source such as XFEL can achieve about 100 W average power output with ~50 μA average current. Applying a conventional adiabatic tapering technique to maximize the output power with a 5 GW seed and 23 m long undulator with parabolically tapered K could possibly increase the efficiency to 18% as shown in figure 2(a), yielding 8 kW average power which is still insufficient to meet industry needs of roughly 20 kW average power.

On the other hand, using a refocused EUV seed to drive a TESSA amplifier, it is possible to convert nearly half of the electron beam power into the 13.5 nm light, all within a 23 m long undulator. The solid lines in figure 2 show the radiation power increase from the starting seed peak power of 5 GW from an upstream FEL to a final >1.8 TW as the electron beam with a modest initial bunching factor of 0.58 is decelerated in the process

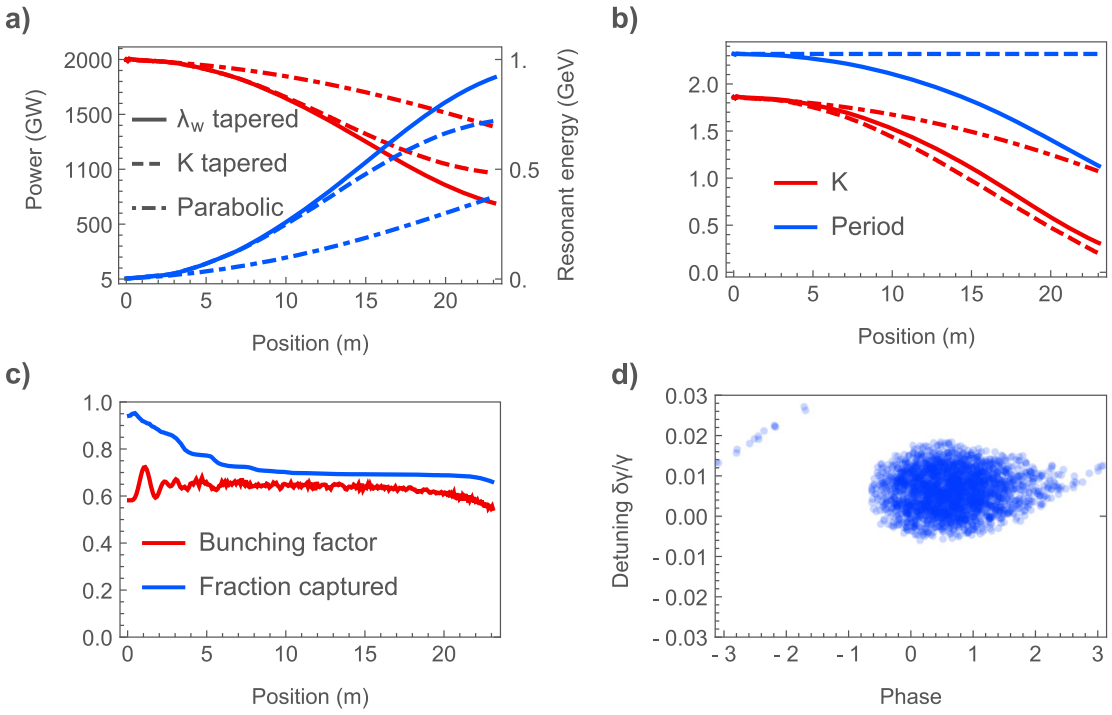

Figure 2. The results of GIT optimizations for a 1 GeV, 4 kA e-beam with a moderate initial bunching factor of 0.58 lasing at 13.5 nm with a seed power of 5 GW from an upstream FEL are shown in the above plots for the case of varying period (solid lines) and constant period (dashed). Also shown are the results of simulations for an undulator with parabolic tapering (dotted–dashed lines). Plot (a) shows the radiation power and resonant energy versus position along the undulator while plot (b) shows the undulator period and strength K for each tapering. Plot (c) shows the bunching and fraction captured along the period-tapered undulator while (d) shows the output longitudinal phase space.

from 1 GeV to 320 MeV for a variable period undulator. Note that this remarkable numerical result still corresponds to a relatively modest decelerating gradient value of about 30 MeV m^{-1}, something that has already been demonstrated experimentally in the inverse (IFEL) configuration.

While the undulator builder equation describes the relationship between period and field amplitude for fixed gap, it is also possible to change the field by increasing the gap while holding the period constant. The results of simulations for a fixed period undulator optimization (dashed curves in figure 2) show a reduced output peak power of 1.35 TW, demonstrating that varying the period of the undulator improves the conversion efficiency as the shorter undulator period results in more total periods.

Applying these results to the same example of a 50 μA average current XFEL-like driver beam (1 GeV electron energy, 20 kHz rep rate, 4 kA peak current, and 500 fs rms bunch length) with the TESSA afterburner, one can achieve >20 kW average power output at 13.5 nm—well within the application target range.

4. X-ray FEL afterburner

In the second example, we consider the application of TESSA tapering to the generation of hard x-rays. The challenge here is to maximize the energy per pulse in order to enable single molecule imaging. More than 10^{13} photons in a >10 fs pulse are required in order to beat the damage and obtain the diffraction information before destroying single molecules [18]. For 4 keV photons (3 Å wavelength), the peak power corresponding to this pulse approaches 1 TW.

We start our simulations with an unbunched electron beam and 5 MW of seeded FEL radiation power, which is typical after self-seeding [19]. An important effect is uncovered by the time-dependent simulations. When trapped in the ponderomotive potential, the electrons undergo synchrotron oscillations in longitudinal phase space with period $z_s = \lambda_w \sqrt{(1 + K^2)/4\, KK_l \cos \psi_r}$ and sideband frequencies are generated as discussed in [4]. In the time-domain, these correspond to oscillations in the time-profile of the field amplitude.

This effect is clear in the simulation results shown in figure 3 where we follow a 5 fs slice of the beam along the undulator. The ripple in the temporal power profile shown in figure 3(b) appears in the spectrum in figure 3(c) as sidebands around the central resonant frequency. As the amplitude of this oscillation grows, particles in those slices experiencing lower laser intensities detrap from the ponderomotive bucket and efficient

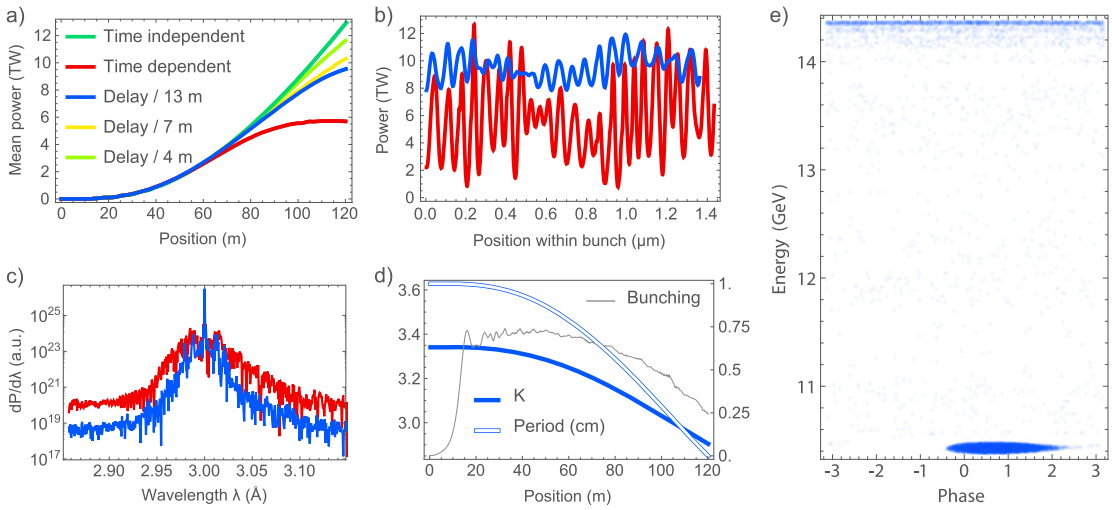

Figure 3. GIT simulations for the case of an x-ray FEL afterburner with a 14.35 GeV, 4 kA unbunched electron beam and 5 MW seed laser with 3 Å wavelength. Shown along the undulator in (a) are the mean powers for simulations with identical initial conditions but different frequencies of chicane delays used to suppress the sideband generation. (b) and (c) show the output temporal profiles and spectra for a standard time dependent simulation and a sideband suppressed simulation with delays every 13 m. The undulator parameters and bunching factor for the case with delays per 13 m are depicted in (d) and output longitudinal phase space is depicted in (e).

Table 1. Simulation parameters.

Parameter	EUV	X-ray
E-beam energy	1 → 0.32 GeV	14.35 → 10.7 GeV
Rms energy spread	0.002	0.0001
E-beam current	4 kA	4 kA
E-beam emittance	2.0 mm mrad	0.3 mm mrad
E-beam spot size	45 μm	10.5 μm
Initial bunching	0.58	shot noise
Laser peak power	5 GW → 1.8 TW	5 MW → 9.6 TW
Laser wavelength	13.5 nm	3.0 Å
Seed Rayleigh range	1 m	3 m
Seed waist	3 m	4 m
Undulator period	2.32 → 1.00 cm	3.34 → 2.90 cm
Undulator K	1.86 → 0.19	3.63 → 2.85
Undulator length	23 m	120 m
Resonant phase	0 → 1.14	0 → 0.66

energy exchange stops. While time independent simulations yield 13 TW of power, the sideband instability limits the average power of time dependent simulations to less than 6 TW as shown in figure 3(a).

This synchrotron sideband instability is somewhat mitigated by strong tapering which causes the synchrotron frequency to quickly vary along the interaction [20]. In order to suppress further the sideband instability, we introduce delay modules periodically throughout the undulator. The function of these delays [21] is to introduce 180° phase shifts for the sideband oscillations while preserving the phase of the fundamental resonant frequency. The required delays are on the order of $z_s(1 + K^2)/4\gamma^2$ or 30–100 nm for our case and can be introduced using magnetic chicanes. Isochronous chicanes are preferred for this application since due to the large energy spread of the electron beam during the deceleration, bunching and trapped fraction are degraded by the introduction of a large chicane dispersion. The number of the chicanes required to suppress the formation of the sidebands is set by the instability growth rate.

Simulations with such delays placed every 13 m (9 delays total) yield more than 11 TW peak power levels and nearly 10 TW average power with 120 m undulator as shown in figure 3 and summarized in table 1. For an 8 fs electron beam 2 times longer than the 4 fs total slippage length, this simulated output power corresponds to $\sim 10^{14}$ photons per pulse. Simulations with more frequent delays, also shown in figure 3(a), further reduce the sideband growth and produce average powers approaching that of time independent simulations.

5. Conclusions

In conclusion, TESSA is a novel approach to convert a significant fraction (nearly 50% in one of our examples) of the energy of a relativistic electron beam into radiation by using tapering optimization techniques developed in the design of high gradient laser accelerators. This paper provides a physical basis for choosing the optimum tapering by dynamically matching the resonant energy gradient set by the undulator to the ponderomotive gradient due to the combined undulator and radiation fields.

The mechanism is ideal for taking advantage of the relatively high wall-plug efficiency of particle accelerators. Maintaining high conversion efficiencies from wall to e-beam to radiation may allow the production of ultra high average power visible light sources with a wide range of applications including fusion science, defense and optically-driven accelerators for high luminosity colliders [22]. In the near term, the single pass efficiency enhancement brought by TESSA can be used to generate high average power EUV light sources and coherent x-ray pulses of unprecedented intensity.

Acknowledgments

The authors are grateful for helpful discussions with Avi Gover, Claudio Emma, Claudio Pellegrini, Juhao Wu, and Gerard Andonian.

References

[1] Bonifacio R, Pellegrini C and Narducci L M 1984 *Opt. Commun.* **50** 373–8
[2] Kroll N M, Morton P L and Rosenbluth M N 1981 *IEEE J. Quantum Electron.* **QE-17** 1436–68
[3] Orzechowski T J *et al* 1986 *Phys. Rev. Lett.* **57** 2172
[4] Jiao Y, Wu J, Cai Y, Chao A W, Fawley W M, Frisch J, Huang Z, Nuhn H-D, Pellegrini C and Reiche S 2012 *Phys. Rev. ST Accel. Beams* **15** 050704
[5] Emma C, Wu J, Fang K, Chen S, Serkez S and Pellegrini C 2014 *Phys. Rev. ST Accel. Beams* **17** 110701
[6] Hafizi B, Ting A, Sprangle P and Tang C M 1988 *Phys. Rev.* A **38** 197
[7] Emma P *et al* 2010 *Nat. Photonics* **4** 641–7
[8] Palmer R 1972 *J. Appl. Phys.* **43** 3014
[9] Duris J, Musumeci P and Li R 2012 *Phys. Rev. ST Accel. Beams* **15** 061301
[10] Duris J *et al* 2014 *Nat. Commun.* **5** 4928
[11] Duris J and Musumeci P 2014 *Proc. Free Electron Laser Conf.* (Switzerland: Basel)
[12] Gover A 2005 *Phys. Rev. ST Accel. Beams* **8** 030701
[13] Musumeci P, Duris J and Murokh A *US Patent (pending)* 61/982623
[14] Gover A, Dyunin E, Lurie Y, Pinhasi Y and Krongauz M V 2005 *Phys. Rev. ST Accel. Beams* **8** 030702
[15] Hemsing E and Xiang D 2013 *Phys. Rev. ST Accel. Beams* **16** 010706
[16] Halbach K 1983 *J. Phys. Colloques* **44** C1–211
[17] Reiche S, Goldhammer K and Musumeci P 2007 *in Proc. of PAC07* (Albuquerque, NM: IEEE)
[18] Chapman D *et al* 1996 *Phys. Med. Biol.* **42** 2015
[19] Amann J *et al* 2012 *Nat. Photonics* **6** 693698
[20] Hafizi B, Ting A, Sprangle P and Tang C M 1988 *Phys. Rev.* A **38** 197
[21] Thompson N R and McNeil B W J 2008 *Phys. Rev. Lett.* **100** 203901
[22] Esarey E, Schroeder C B and Leemans W P 2009 *Rev. Mod. Phys.* **81** 1229–85